

Measurement of higher-order stress-strain effects in granular materials undergoing non-uniform deformation

Matthew R. Kuhn^{a,*}, Ching S. Chang^b

^a*Br. Godfrey Vassallo Prof. of Engrg., Donald P. Shiley School of Engrg., Univ. of Portland, 5000 N. Willamette Blvd., Portland, OR 97231, USA*

^b*Dept. of Civil and Env. Engrg., University of Massachusetts, Amherst, MA 01002, USA*

Abstract

Discrete element (DEM) simulations demonstrate that granular materials are non-simple, meaning that the incremental stiffness of a granular assembly depends on the gradients of the strain increment as well as on the strain increment itself. In quasi-static simulations, two-dimensional granular assemblies were stiffer when the imposed deformation was non-uniform than for uniform deformation. The contacts between particles were modeled as linear-frictional contacts with no contact moments. The results are interpreted in the context of a higher-order micro-polar continuum, which admits the possibility of higher-order stress and couple-stress. Although the behavior was non-simple, no evidence was found for a couple-stress or an associated stiffness. The experimental results apply consistently to three particle shapes (circles, ovals, and a non-convex cluster shape), to assemblies of three sizes (ranging from 250 to 4000 particles), and at pre-peak and post-peak strains.

Keywords: Granular material, micro-polar continua, plasticity, incremental response, stiffness, discrete element method

1. Introduction

Large solid regions are commonly modeled as homogeneous continua, ignoring the underlying heterogeneity that may exist at a smaller scale and, in the case of granular materials, also ignoring the discontinuous nature of the micro-scale movements. Any continuum model of a large macro-region requires the choice of a continuum class and of a constitutive form. The most common continuum class is a classical, Cauchy continuum, in which the internal force and deformation quantities are the conventional stress and strain. Micro-morphic continua, such as a Cosserat continua, are examples of non-classical continua in which the conventional strain at a material point is augmented with other kinematic quantities (micro-rotation, micro-stretch, higher-order micro-strains, etc.), and the conventional stress is augmented by corresponding, conjugate quantities (couple-stress, higher-order stress, etc.) [12, 17], see e.g. [3] for a perspective on the origin of such non-local theories. The

*Corresponding to: Donald P. Shiley School of Engineering, University of Portland, 5000 N. Willamette Blvd., Portland, OR, 97203, USA. Email: kuhn@up.edu

Email addresses: kuhn@up.edu (Matthew R. Kuhn), chang@ecs.umass.edu (Ching S. Chang)

Preprint submitted to Elsevier

March 25, 2021

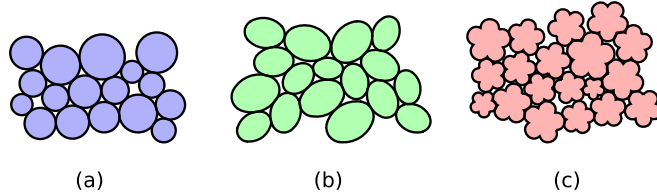


Figure 1: Three particle shapes used in the simulations: circles, ovals, and nobbies.

most common constitutive form is that of a simple material, in which stress at a continuum point depends upon the history of the local strain and its rate at the point. With non-simple materials, such as second-gradient materials [13], the stress at a material point depends on the local gradients of strain. Non-simple materials also include non-local media in which stress at a point depends on the deformation within a small region around the point.

With granular materials, the issue of a proper continuum treatment at the macro-scale is of particular importance, because heterogeneity is inherent and pervasive and can occur at a scale that is significant when compared with a specimen's size [7, 16, 21, 15]. Moreover, the strength of a granular material is not only affected by heterogeneity, but strength is largely a bulk expression of material behavior within localized deformation features such as shear bands, compression bands, and micro-bands [4, 9, 22, 11, 14]. As a consequence, the observed mechanical behavior of a specimen, particularly during post-peak softening, is likely affected by the size of the specimen relative to that of its localization features. The view of granular materials as simple materials has already been called into question by experiments that demonstrate an effect of the gradients of shearing strain on the shear stress [8].

The paper presents evidence of non-simple and size-dependent behavior during compression and extension loading, and it is organized in the following manner. We begin by describing DEM experiments, in which small rectangular assemblies are deformed either uniformly or in a non-uniform manner. The breadth of these assemblies is similar to the observed thickness of shear bands. We then present a continuum framework for interpreting the stress-response to the imposed deformations — a generalized micro-morphic continuum — and a consistent set of stress measures that apply to discrete, granular media. We then analyze the simulation results, determining whether assembly size affects the stress-response, whether the results support a Cosserat approach with couple-stress, and whether the stress-strain response depends upon the gradients of strain.

2. Experiments

Two series of slow, quasi-static discrete element (DEM) simulations were conducted on square two-dimensional assemblies of particles of three different shapes: circles, ellipse-like ovals, and composite non-convex “nobby” shapes that were formed from five satellite circles arranged around a central circle (Fig. 1). Simulations with the non-circular particles were intended to examine possible micro-polar effects that have been conjectured to result from elongated shapes or from particle pairs that share multiple contacts [5]. Briefly, the two series of simulations were incremental loadings of the two types shown in Fig. 2: (a) increments of uniform horizontal biaxial compression/extension, and (b) increments in which a non-uniform bending-type deformation was intentionally imposed. By comparing the two series

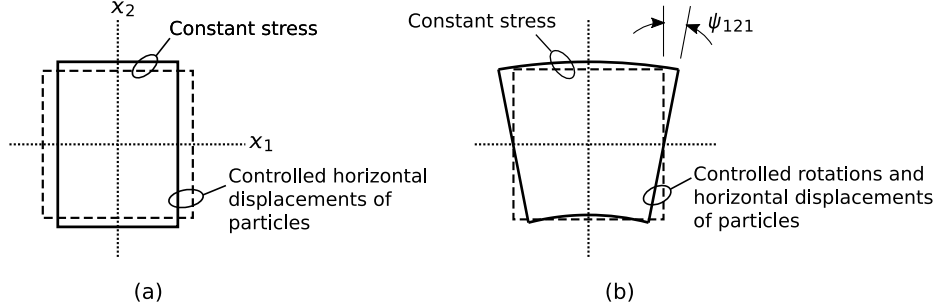


Figure 2: Two series of incremental loadings of particle assemblies: (a) uniform biaxial compression and extension; (b) non-uniform deformation with tilting side boundaries.

of experiments, we determined the incremental effects of higher-order gradients of the displacement field (i.e. gradients of strain) and of the rotation field. These two series of incremental simulations were conducted after an initial stage of nearly uniform biaxial compression that brought the assemblies to four different initial strain levels, including zero strain, two strains at and beyond the condition of peak stress, and strain at the post-peak critical state.

As a final variable in the simulations, we conducted simulations on assemblies of different sizes, ranging from assemblies of only 256 particles to assemblies of over 4,000 particles. The stress-strain behavior of such small assemblies, even those with thousands of particles, can be quite erratic and can be sensitive to the initial particle arrangement [10], so we conducted simulations on multiple (as many as 300) initial assemblies of a given size and then averaged the results. To summarize, variations in the simulations allowed us to determine the effects of non-uniform strain (and rotation) on the incremental stiffnesses of two-dimensional assemblies and the effects of the three following variables: particle shape, assembly size, and initial loading strain.

All simulations began with dense isotropic random arrangements of particles that were contained within periodic boundaries. The particle sizes, regardless of shape, were poly-disperse, with a size range of $0.56D$ to $1.7D$, where D is the mean size. The oval particles had a length/width aspect ratio of 1.30, and the nobby particles were distinctly non-convex, so that two neighboring particles could touch at one, two, or three points. Linear-frictional contacts were used, with equal normal and tangential stiffnesses k and a friction coefficient $\mu = 0.50$. No contact moments were applied in the simulations. Both series of the incremental tests in Fig. 2 followed an initial stage of biaxial compression, in which the horizontal width of an assembly was reduced at a constant rate while maintaining a constant vertical stress σ_{22} . Periodic boundaries were used throughout this initial loading stage. Figure 3 shows the results of the initial loading and the four strains at which the two series of incremental simulations were conducted.

The series of non-uniform “bending” simulations in Fig. 2b could not be conducted with periodic boundaries, so after the initial stage of biaxial compression, an assembly’s periodic boundaries were removed and replaced with an irregular “flexible” boundary that passed from center to center of the peripheral particles around an assembly’s perimeter. This process, an alternative to using flat platens, creates assemblies in which the particles retain their initial arrangement, with a fabric and stress that is nearly the same as during the preceding loading

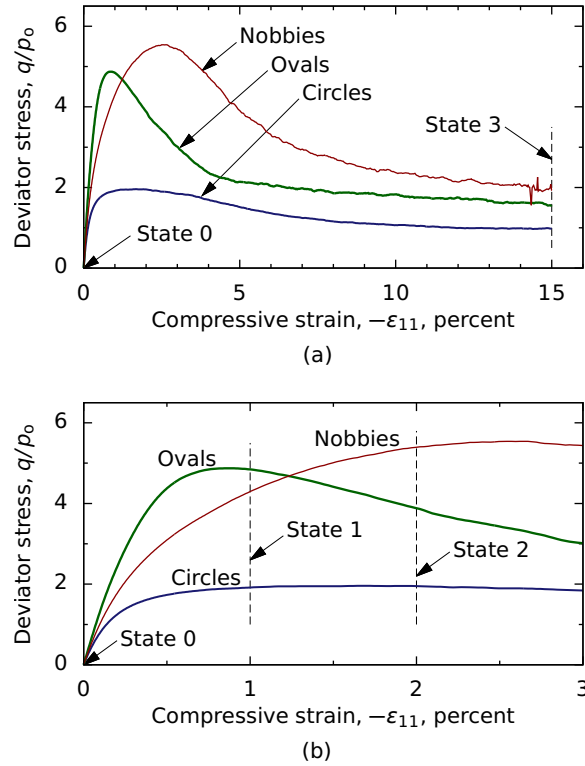


Figure 3: Stress and strain for the initial phase of monotonic biaxial compression with constant lateral stress. The incremental response to a non-uniform deformation field was measured at four states of strain.

stage. Both series of incremental simulations in Fig. 2 were then conducted with flexible boundaries.

After the initial stage of loading to a particular strain state, the first series of simulations, shown in Fig. 2a, were of conventional biaxial compression and extension: each assembly was horizontally compressed (or extended) between its two sides of boundary particles, which approached (or retracted) at a constant rate of strain, while maintaining a constant stress along the upper and lower sides. These simulations were performed to determine the incremental Young's modulus E for conditions of loading and unloading, and they provide a benchmark against which the second series of tests can be compared. In a sense, the incremental simulations were a continuation of the initial monotonic loading, although with flexible rather than periodic boundaries. As will be seen, the non-uniform "bending" experiments of Fig. 2b induced unloading within a part of an assembly, so we also conducted the incremental *extension* simulations to determine the unloading modulus.

The second series of experiments were special bending tests, in which the left and right sides of an assembly (i.e., chains of particles) were rotated as shown in Fig. 2b. To induce these conditions, particles along the left and right sides were displaced horizontally and were forced to corotate with their boundary. These tests provide a means of measuring the material response to imposed gradients of strain and of particle rotation. As with the compression tests, a constant stress was maintained along the top and bottom boundaries during the

bending tests.

In both the compression and bending series of simulations, the top and bottom boundaries were flexible, with a uniform vertical pressure applied to virtual links that joined the centers of neighboring peripheral boundary particles, in the manner of a flexible membrane in geotechnical testing. The peripheral particles along these boundaries could freely move and rotate under the influence of a constant boundary stress σ_{22} applied at the particles' centers (see [1] for the first known use of such boundaries). Along the left and right boundaries in both sets of experiments, the vertical movements of particles were unconstrained, but the horizontal movement u_1^p and rotation θ_3^p of each “ p ” particle was constrained to conform with an average strain ε_{11} and an average strain gradient ψ_{112} :

$$du_1^p = d\varepsilon_{11}x_1^p + d\psi_{112}x_1^px_2^p \quad (1)$$

$$d\theta_3^p = -d\psi_{112}x_1^p \quad (2)$$

where $d\varepsilon_{11}$ is the conventional horizontal strain increment, $d\psi_{112}$ is the vertical gradient of the horizontal strain, and x_i^p is the location of boundary particle p 's center. In Eq. (1), the deformation $d\psi_{112}$ is the second-gradient of displacement, $du_{1,12}$, applied at the boundaries. We emphasize that Eqs. (1)–(2) are the imposed conditions along the side boundaries, but the two deformations, $d\varepsilon_{11}$ and $d\psi_{112}$, can also be considered “macro-strains”: characteristic strains within a non-homogeneous micro-region that constitutes a representative volume element (RVE, Section 3). To constrain the movements and rotations of the side particles, restraining forces and moments were applied to the centers of these boundary particles. The combined effect of these external forces and moments can be computed as equivalent “bending moments” applied to the left and right sides, as will be discussed later. Unlike the side particles, the assembly's interior particles were free to both move and rotate, as they accommodated the imposed boundary conditions.

With each simulations in Fig. 2, our intent was to determine the stress response of a granular RVE that was freely responding to a small, incremental deformation. Because rotations and movements were imposed upon those particles along the sides of an assembly and constant force was applied to those particles along the top and bottom, these boundary particles are not considered part of a “freely responding” RVE (Fig. 4a). For this reason, we measured the response of an interior sub-assembly that was fully contained within (and surrounded by) the boundary particles (Fig. 4b). The manner in which stress was computed within this freely responding sub-assembly is described in the next section, which also describes two variations of analyzing the sub-assemblies depicted in Fig. 4b. Note that stress and deformation are computed within sub-assemblies that contain fewer particles than the full assembly: the assemblies of 256, 1024, and 4096 particles encompassed sub-assemblies of about 180, 900, and 3800 particles, respectively.

3. Generalized continuum setting

We computed various stress quantities within the assemblies by taking the theoretic approach advocated by Germain [6], in which movements and strains are accepted as the privileged, fundamental quantities, and stresses, in their various forms, are merely derived as conjugates to these movements and strains. If the operative displacement quantities *at a continuum point* are those of a generalized, micro-polar continuum and are taken as the displacement gradient $\delta u_{i,j}$, second gradient $\delta u_{i,jk}$, micro-rotation $\delta\theta_i$, and micro-rotation

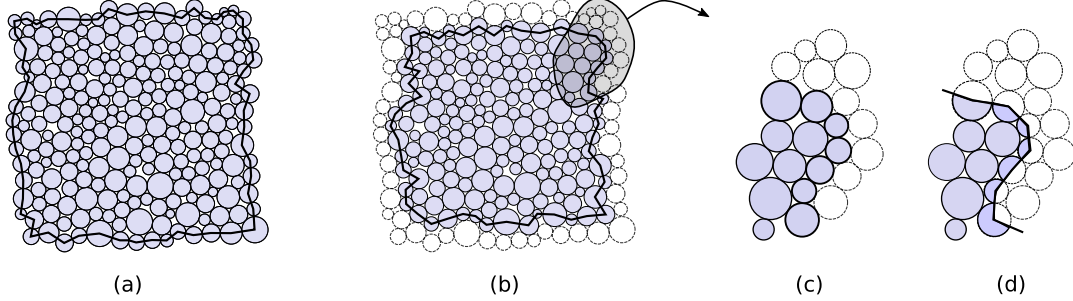


Figure 4: Alternative RVEs within an assembly of 256 disks: (a) assembly of all disks, noting that the movements of side particles were imposed; and (b) sub-assembly for computing the response of a freely responding RVE. These sub-assemblies were used to measure the stress-response in the paper. For the sub-assembly, two RVE boundaries are possible: (c) boundary fully encompassing the peripheral particles, and (d) boundary passing through the centers of peripheral particles.

gradient $\delta\theta_{i,j}$, then the internal virtual work δW^a that is formed from these quantities is (see [2])

$$\delta W^a = \sigma_{ji}\delta u_{i,j} + \sigma_{jki}\delta u_{i,jk} + T_i\delta\theta_i + T_{ji}\delta\theta_{i,j} \quad (3)$$

In this expression of virtual work, force quantity σ_{ji} is immediately recognized as the stress, as it is conjugate with the displacement gradient, although the equation imposes no condition of symmetry on this stress. The other force quantities are the higher-order stress σ_{jki} and the internal torque and internal torque-stress, T_i and T_{ij} . Although no continuum internal torques T_i apply in our simulations, the higher-order stress and torque stress were measured in a manner that is described later. The internal virtual work of Eq. (3) can be rearranged to yield the more familiar form of a higher-order Cosserat continuum:

$$\delta W^b = \sigma_{ji}(\delta u_{i,j} + e_{ijk}\delta\theta_k) + \sigma_{jki}(\delta u_{i,jk} + e_{ij\ell}\delta\theta_{\ell,k}) + \mu_{ji}\delta\theta_{i,j} \quad (4)$$

where we have introduced the couple-stress μ_{ji} , which is complementary with the gradient of the micro rotation $\delta\theta_{i,j}$. Stress σ_{ji} can be asymmetric, and its non-symmetric part is complementary with the difference between micro-rotation $\delta\theta_k$ and the asymmetric part of the displacement gradient $\delta u_{i,j}$. The virtual works of Eqs. (3) and (4) are equivalent, so that the couple-stress, torque-stress, and higher-order stress are related, as

$$\mu_{ji} = T_{ji} - e_{k\ell i}\sigma_{\ell jk} . \quad (5)$$

The stress quantities in Eqs. (3)–(5) apply to a point within a continuum. When the continuum is intended to represent a discrete, granular material, we use the superscript “0” to designate the *macro-stress* of a small granular region (i.e., a *micro-region* or RVE) that is representative of a continuum point [2]. That is, macro-stresses are the representative stresses of a small granular region rather than of a continuum point or even of a point within an individual particle inside the region.

The various macro-stresses are measured for a micro-region — an aggregate of discrete granular constituents which forms the RVE of a continuum point. The macro-stresses that arise from the continuum settings of Eq. (3) and (4) can be computed within a granular micro-region \mathcal{B} from summations of contact forces and contact moments, so that the virtual works

of the continuum stresses and of the macro-stresses coincide (see [2]). Each macro-stress is computed from the contact forces, with either of two alternative sums. One sum involves the contacts $b \in \partial\mathcal{B}$ between peripheral, boundary particles and the RVE's exterior; the second sum is of the contacts c among the interior and boundary particles. The alternative expressions, using either the boundary contacts or all contacts, are as follows:

$$\sigma_{ji}^0 = \frac{1}{V} \sum_{b \in \partial\mathcal{B}} f_i^b x_j^b = \frac{1}{V} \sum_{c \in \partial\mathcal{B} \cup \mathcal{B}} f_i^c l_j^c \quad (6)$$

$$\sigma_{jki}^0 = \frac{1}{2V} \sum_{b \in \partial\mathcal{B}} f_i^b x_j^b x_k^b = \frac{1}{2V} \sum_{c \in \partial\mathcal{B} \cup \mathcal{B}} f_i^c J_{jk}^c \quad (7)$$

$$\begin{aligned} \mu_{ji}^0 &= \frac{1}{V} \sum_{b \in \partial\mathcal{B}} \left(m_i^b x_j^b - \frac{1}{2} e_{ikl} f_k^b x_l^b x_j^b \right) \\ &= \frac{1}{V} \sum_{c \in \partial\mathcal{B} \cup \mathcal{B}} \left[m_i^c l_j^c + e_{ikl} f_k^c \left(\frac{1}{2} J_{lj}^c - x_l^c l_j^c \right) \right] \end{aligned} \quad (8)$$

$$\begin{aligned} T_{ji}^0 &= \frac{1}{V} \sum_{b \in \partial\mathcal{B}} m_i^b x_j^b \\ &= \frac{1}{V} \sum_{c \in \partial\mathcal{B} \cup \mathcal{B}} [m_i^c l_j^c + e_{ikl} f_k^c (J_{lj}^c - x_l^c l_j^c)] \end{aligned} \quad (9)$$

In these expressions, f_i^b are external boundary forces applied to the peripheral particles of a micro-region; f_i^c are internal contact forces between particles within the region and external contact forces between peripheral particles and the region's exterior; m_i^b and m_i^c are boundary moments and contact moments; l_j are branch vectors that join the centers of contacting particle pairs or join the centers of peripheral particles and exterior contact points; x_j^b and x_j^c are the locations of external forces or of internal contacts; and tensors J_{jk}^c are the quadratic differences $x_j^q x_k^q - x_j^p x_k^p$ for two contacting particles, p and q , or for peripheral particles and their exterior contacts. In a two-dimensional setting, V is the RVE area; with three-dimensional RVEs, V is the volume. Each equation gives two summations for a macro-stress quantity: the first summation is of peripheral contacts “ b ” along the boundary $\partial\mathcal{B}$ of region \mathcal{B} ; whereas, the second summation is of contacts “ c ” both within the region and between the region and its exterior, $c \in \partial\mathcal{B} \cup \mathcal{B}$. Because the DEM algorithm uses a relaxation technique that only achieves an approximate equilibrium, the external and internal sums in Eqs. (6)–(9) were not precisely equal, but they never differed by more than 0.1%.

As was described in Section 2, Fig. 4b depicts a sub-assembly RVE that is surrounded by an external layer of particles whose movements and rotations (or external forces) were controlled during a simulated increment of deformation, as in Eqs. (1)–(2). The expressions of macro-stress in Eqs. (6)–(9) suggest two approaches to computing stress within a sub-assembly RVE, which are illustrated in Figs. 4c and 4d. Both figures show three sets of particles: unshaded external particles that are outside the RVE, peripheral particles of the RVE, and interior particles fully inside the RVE. With the variant of Fig. 4c, the RVE fully encompasses the peripheral particles; whereas, the boundary of the RVE in Fig. 4d passes through the peripheral particles but includes the interior portions of these particles along with the contacts between the peripheral and other RVE particles.

Eqs. (6)–(9) apply differently to the two boundary variants in Figs. 4c and 4d. With Fig. 4c,

the boundary forces and moments, f_i^b and m_i^b , are the contact forces and moments between the peripheral and external particles. Because no contact moments were present in our simulations, the torque-stress T_{ji}^0 is zero [2]. Moreover, the contribution $e_{ik\ell} f_k^b x_\ell^b x_j^b$ in Eq. (8) is zero for two-dimensional assemblies (see Eq. 13 below), so the couple-stress μ_{ji}^0 in Eq. (5) is also zero. The situation is different for the RVE in Fig. 4d. Boundary forces and moments, f_i^b and m_i^b , are applied to the bodies of peripheral particles, as these body forces must balance the contact forces between the peripheral and interior RVE particles. For this choice of boundary, the moments m_i^b are not necessarily zero, and as a result, torque-stresses and couple-stresses can arise with this RVE.

4. Results

Our simulations were intended to measure the *incremental* macro-stress response to small deformation increments: specifically, the increments $d\varepsilon_{11} = du_{1,1}$ and $d\psi_{112} = du_{1,12}$ (see Eqs. 1 and 2). Two factors must be considered when computing the incremental response of an assembly in the context of the macro-stresses of Eqs. (6)–(9). First, it is clear from the external contact expressions for σ_{jki}^0 and μ_{ji}^0 , which contain the products $x_j x_i$, that these two macro-stresses depend upon the size of the micro-region that is being considered: doubling the assembly size will double the contributions of these products to their macro-stresses (for example, with the first stress measure in Eq. 7, doubling a 2D assembly’s length and width but maintaining the same particles’ sizes will double the number of particles along the assembly’s perimeter, quadruple the area A , and quadruple the $x_i^b x_j^b$ products, thus increasing σ_{jki}^0 by a factor of two). Second, the incremental stiffness moduli of an assembly (micro-region) will depend upon (and will be roughly proportional to) the contact stiffness, k , between particles. To analyze the results of our two-dimensional simulations in a consistent, size-independent manner, we normalized the results with the following dimensionless stiffness moduli:

$$K_\varepsilon = \frac{1}{k} (d\sigma_{11}^0/d\varepsilon_{11}) \quad (10)$$

$$K_\psi = \frac{2}{k} (d\sigma_{121}^0/d\psi_{121}) \frac{A}{I_{22}} \quad (11)$$

$$K_\theta = \frac{1}{k} (dT_{13}^0/d\theta_{3,1}) \frac{A}{I_{22}} = K_\varepsilon \frac{A}{I_{22}} \ell^2 \quad (12)$$

where we explicitly represent the volume V of a two-dimensional assembly as its area A . These three moduli are the stiffnesses associated with the first, second, and fourth terms on the right of Eq. (3). (In a three-dimensional setting, each modulus would be divided by a micro-scale measure with dimensions of length, for example, the mean particle size D , to maintain a dimensionless character.) Note that the experiments are limited to determining three of the many moduli that are associated with stresses σ_{ij}^0 , σ_{ijk}^0 , and T_{ij}^0 , and further experiments would be required for examining the other moduli (see [18, 19]).

The first modulus, K_ε , is simply the normalized Young’s modulus that we measured with the series of incremental biaxial compression and extension tests with constant lateral stress (see Fig. 2a).

The modulus K_ψ is the Young’s modulus of a two-dimensional linear-elastic rectangular solid undergoing non-uniform deformation, as derived by treating the rectangle as an Euler–Bernoulli beam, where $d\psi_{121}$ is the beam’s curvature (Fig. 5a), and $I_{22} = \int x_2 x_2 dA$ is the

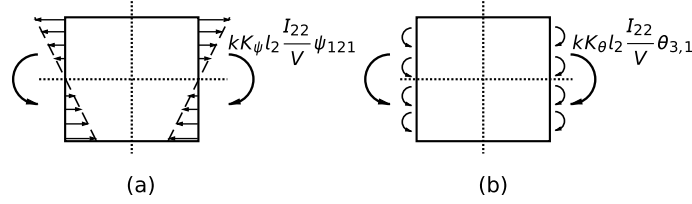


Figure 5: Stiffnesses attributed to boundary forces and moments: (a) the strain gradient $d\psi_{121} = du_{1,21}$ produces non-uniform side forces with associated stiffness K_ψ ; (b) the rotation gradient $d\theta_{3,1}$ produces side moments with associated stiffness K_θ . Parameter l_2 is the assembly height.

second-moment of the assembly's volume measured about the x_1 axis. If the material is simple, such that stress is independent of the gradients of strain, then the two moduli, K_ε and K_ψ , will be equal.

The third modulus K_θ is the stiffness associated with the applied boundary torques that are required to rotate particles along the side boundaries (Fig. 5b). This modulus is that of an elastic two-dimensional Cosserat plate, in which rotational stiffness is exclusively derived from the couple-stress [20]. This rotation stiffness is commonly expressed as the product of the Young's modulus and a squared measure of micro-mechanical length ℓ .

A fourth stiffness is associated with the couple-stress μ_{13} , noting the relationship in Eq. (5),

$$K_\mu = \frac{1}{k} \left(d\mu_{13}^0 / d\theta_{3,1} \right) \frac{A}{I_{22}} \quad (13)$$

$$= K_\theta + \frac{1}{k} \left(d\sigma_{312}^0 / d\theta_{3,1} - d\sigma_{213}^0 / d\theta_{3,1} \right) \frac{A}{I_{22}} \quad (14)$$

In our two-dimensional setting, the stresses σ_{312}^0 and σ_{213}^0 are zero, so that moduli K_μ and K_θ are equivalent. Only the latter is reported below.

The stiffnesses in Eqs. (12) and (13) can be measured with either of the two types of RVE boundaries illustrated in Figs. 4c and 4d, by computing the small changes in the various stresses that resulted from the displacement probes of the two series of simulations (see Figs. 2a and 2b). We found that the two types of boundaries gave nearly identical results, and only the results with the boundaries shown in Fig. 4d are reported herein.

4.1. Response to biaxial compression and extension

Recall that our incremental simulations followed periods of sustained, monotonic horizontal biaxial compression. Our primary interest is the response of assemblies to the non-uniform "bending" deformation of Fig. 2b, but we also conducted simulations of increments of biaxial compression and extension (Fig. 2a), as these simulations will serve as the reference condition with which the response to non-uniform deformation is compared. The non-uniform simulations of Fig. 2b produced horizontal compressive loading in the lower half of the assembly while producing a reversed, extensional increment in the upper half (Fig. 2b), calling for both biaxial compression and biaxial extension simulations to serve as dual reference conditions. The normalized compression and extension moduli are designated as $K_\varepsilon^{\text{load}}$ and $K_\varepsilon^{\text{unload}}$.

Table 1: Moduli K_ε for incremental loading and unloading of assemblies of 1024 particles.

Shape	Strain	$K_\varepsilon^{\text{load}}$	$K_\varepsilon^{\text{unload}}$
Circles	0%	0.855	0.855
	1%	0.181	0.425
	2%	0.173	0.335
	15%	0.003	0.212
Ovals	0%	1.550	1.550
	1%	0.823	1.067
	2%	0.715	0.695
	15%	0.057	0.438
Nobbies	0%	1.095	1.095
	1%	0.119	0.958
	2%	0.052	0.867
	15%	0.046	0.476

Table 2: Effect of assembly size on modulus K_ε for assemblies at 1% strain.

Shape	Size	$K_\varepsilon^{\text{load}}$	$K_\varepsilon^{\text{unload}}$
Circles	256	0.280	0.542
	1024	0.181	0.425
	4096	0.107	0.396
Ovals	256	0.953	1.072
	1024	0.823	1.067
	4096	0.585	1.102
Nobbies	256	0.117	1.106
	1024	0.119	0.958
	4096	0.110	0.884

Table 1 presents K_ε values for the three particle shapes at four different strains for the assemblies containing 1024 particles. As would be expected, the normalized Young's modulus K_ε , measured with increments of biaxial compression, decreases with increasing strain, as the material softens with continued loading. The loading modulus was smallest for disks and largest for the assemblies with oval particles. The fact that the stiffness is greater for ovals than for the non-convex nobbies indicates that particle elongation (non-sphericity) has a greater stiffening effect than particle non-convexity (a type of angularity). The figure also gives the unloading moduli that were measured with increments of biaxial extension. As would be expected during strain hardening, the unloading modulus is typically larger than the loading modulus. The difference is most pronounced for the nobbies and is least apparent with ovals. The degradation of the unloading modulus is largely due to a loss of inter-particle contacts, as our assemblies dilated during the initial phase of monotonic loading.

The effect of assembly size is shown in Table 2, which gives the moduli K_ε for three assembly sizes at a common strain of 1%. Stiffness, whether for loading or unloading, generally

decreases with assembly size, a result observed at three strains: 1%, 2%, and 15%. Apart from an inherent size-effect, this result could be due, in part, to differences in the fabrics of the differently sized assemblies. The process of creating the initial assemblies — fitting them into a small periodic box — produces different densities of contacts, depending upon the numbers of particles in the original assembly. Because each additional contact brings an increase in assembly stiffness, we should adjust the stiffnesses in Table 2 by dividing by the corresponding contact densities (numbers of contacts divided by assembly volume). With this adjustment, the unloading modulus $K_\varepsilon^{\text{unload}}$ was nearly constant for the three assembly sizes, but the loading modulus $K_\varepsilon^{\text{load}}$ still exhibited the same trend of a decrease in stiffness with increasing assembly size.

4.2. Response to non-uniform deformation and rotation

With the simulations of non-uniform deformation (Fig. 2b), we sought answers to two questions. First, we determined whether a stiffness K_θ is associated with torque-stress (or couple-stress) for a granular material subject to a field of non-uniform micro-rotation, $\theta_{3,1}$. The presence of such stiffness is central to modeling granular materials as Cosserat continua. Second, we determined whether stiffness is greater for conditions of non-uniform deformation, with $du_{1,12} \neq 0$, than for uniform deformation. We note that the possibility of a non-symmetric stress, with $\sigma_{12} \neq \sigma_{21}$, could not be resolved with these simulations, due to symmetry of the loading about the x_1 (Fig. 2b).

In regard to the first question, by applying the displacements and rotations of Eqs. (1) and (2), we produced increments of non-uniform strain and rotation within the assemblies. These constraints on displacement and rotation were applied to the side boundaries (the unshaded side particles in Fig. 4b), while the stress and the average deformation and rotation fields were computed for the interior particles (the shaded RVE particles in Figs. 4b–4d). We found that the average rotation gradient of the interior particles, $d\theta_{3,1}$, was consistent with the imposed deformation gradient $d\psi_{112}$ that was applied at the boundary, and the measured internal gradient $d\theta_{3,1}$ was typically within 10% of $d\psi_{112}$. As was explained in the previous section, a subtle difference in the side boundaries will either admit or abrogate moments m_3 among the peripheral particles. If the RVE of Fig. 4c is used, the moments are zero, the torque-stress T_{13} is zero, modulus K_θ is zero, and the micro-mechanical length scale ℓ is zero. On the other hand, boundary moments can exist and can be measured with the RVE illustrated in Fig. 4d, for which body moments arise to provide moment equilibrium for the peripheral particles. We found, however, that even in the presence of a rotation gradient $d\theta_{3,1}$, the average torque-stress T_{13} was nearly zero for the RVE with body moments. That is, although these moments were present along an assembly’s peripheral particles, they nearly canceled each other, leaving a net torque-stress T_{13} close to zero. This observation was determined for all particle shapes, all assembly sizes, and at all strains: the stiffness K_θ in Eq. (12) was typically less than 0.001. These small values correspond to a micro-mechanical length ℓ that is much smaller than the mean particle size — a length scale smaller than the grains themselves. Because this result applies to all three particle shapes, we conclude that a micro-rotation stiffness is not induced by multiple inter-particle contacts (as with the nobby shapes) or by an elongated particle shape (as with ovals).

To address the second question — whether stress is independent of strain gradients — we measured the normalized modulus K_ψ in Eq. (11). This modulus is the Young’s modulus that would be consistent with a simple linear-elastic plate, in which stiffness is *independent* of any gradients of strain. If the response of an assembly depends only on the strain ε_{11} and

Table 3: Comparison of stiffness, K_ε and K_ψ , for biaxial and bending types of deformation, for assemblies of 1024 particles.

Shape	Strain	$\frac{1}{2}(K_\varepsilon^{\text{load}} + K_\varepsilon^{\text{unload}})$	K_ψ
Circles	0%	0.855	0.806
	1%	0.303	0.547
	2%	0.254	0.398
	15%	0.107	0.284
Ovals	0%	1.550	1.554
	1%	0.945	1.215
	2%	0.704	0.756
	15%	0.248	0.427
Nobbies	0%	1.095	1.035
	1%	0.538	0.720
	2%	0.459	0.777
	15%	0.261	0.367

is independent of the strain gradient $d\psi_{112}$, the two moduli, K_ε and K_ψ , will be equal. We note, however, that particles in the upper and lower halves of an assembly are subject to increments of horizontal tension and compression, respectively (see Fig. 5a), and we must account, of course, for the different moduli — $K_\varepsilon^{\text{load}}$ and $K_\varepsilon^{\text{unload}}$ — that apply to the lower and upper parts of an assembly. That is, we should compare modulus K_ψ with the *average* of the two incremental stiffnesses, $K_\varepsilon^{\text{load}}$ and $K_\varepsilon^{\text{unload}}$, since the two stiffnesses apply to equal volumes of material.

These comparisons are made in Table 3 for assemblies of three particle shapes and at four strains. Except at the start of loading (state 0 in Fig. 3), the modulus K_ψ is consistently larger than the averaged modulus K_ε : the Young’s modulus of a granular material is larger for conditions of non-uniform deformation than for uniform biaxial loading. This experimental result demonstrates that granular materials are non-simple — that the stress depends upon the strain gradients and not solely on the strain — and that a non-simple constitutive form should be adopted for granular materials.

Table 4 gives the higher-order modulus K_ψ for assemblies of three sizes: 256, 1024, and 4096 particles. The results are the incremental stiffnesses for assemblies that were pre-loaded to a strain of 1% (state 1, Fig. 3). For all three particle shapes and all assembly sizes, the modulus K_ψ is larger than the averaged Young’s modulus K_ε . The ratio of the two moduli, K_ψ/K_ε , is largest for the assemblies of disks and smallest for the oval assemblies. Moreover, for each particle shape, the ratio is about the same for all three assembly sizes. One might think that the effect of assembly size should diminish with increasing size, but recall that with each assembly size, we imposed boundary conditions that produced a uniform *gradient* of strain across an assembly’s full height — regardless of the number of particles in the height — and the results show that stiffness is augmented by the presence of this strain gradient, independent of the assembly size.

Table 4: Effect of assembly size on moduli K_ϵ and K_ψ for assemblies at 1% strain.

Shape	Size	$\frac{1}{2}(K_\epsilon^{\text{load}} + K_\epsilon^{\text{unload}})$	K_ψ
Circles	256	0.411	0.675
	1024	0.303	0.547
	4096	0.252	0.444
Ovals	256	1.012	1.334
	1024	0.945	1.215
	4096	0.843	1.087
Nobbies	256	0.612	0.832
	1024	0.538	0.720
	4096	0.497	0.673

5. Conclusions

The experiments reveal evidence of an internal length-scale for granular materials. This result is manifest in the effect of assembly size on the loading stiffness: larger assemblies exhibit softer behavior. Although this size effect is absent at the start of loading and in the unloading modulus (after adjusting for contact density), the stiffer loading behavior of small samples suggests that some form of length-scale is operative. But how should one model this effect? The measured absence of a Cosserat stiffness — a stiffness associated with the spatial gradient of micro-scale rotation — should discourage the use of micro-polar continuum models for granular materials. On the other hand, we found that granular assemblies are much stiffer when subject to a non-uniform deformation field than would be predicted with a simple size-independent Young’s modulus. Moreover, this increase in stiffness for non-uniform loading conditions was nearly independent of the assembly size, provided that the imposed second gradient of displacement (i.e., first gradient of strain) was the same for each sample size. These conclusions have only been tested for two-dimensional granular materials, for a simple linear-frictional contact type, and for three particle shapes, but the results clearly suggests that a length-scale should be directly incorporated within the constitutive form: that granular materials should be modeled as non-simple materials, in which stress and stiffness depend upon both strain and the gradients of strain.

References

- [1] J. P. Bardet, J. Proubet, A numerical investigation of the structure of persistent shear bands in granular media, *Géotechnique* 41 (4) (1991) 599–613.
- [2] C. S. Chang, M. R. Kuhn, On virtual work and stress in granular media, *Int. J. Solids Struct.* 42 (13) (2006) 6026–6051.
- [3] F. Dell’Isola, U. Andreaus, L. Placidi, At the origins and in the vanguard of peridynamics, non-local and higher-gradient continuum mechanics: An underestimated and still topical contribution of gabrio piola, *Math. and Mech. of Solids* 20 (8) (2015) 887–928.
- [4] J. Desrues, R. Chambon, M. Mokni, F. Mazerolle, Void ratio evolution inside shear bands in triaxial sand specimens studied by computed tomography, *Géotechnique* 46 (3) (1996) 529–546.
- [5] F. Froio, G. Tomassetti, I. Vardoulakis, Mechanics of granular materials: The discrete and the continuum descriptions juxtaposed, *Int. J. Solids Struct.* 43 (25–26) (2006) 7684–7720.
- [6] P. Germain, The method of virtual power in continuum mechanics. part 2: Microstructure, *SIAM J. on Appl. Math.* 25 (3) (1973) 556–575.
- [7] M. R. Kuhn, Heterogeneity and patterning in the quasi-static behavior of granular materials, *Granul. Matter* 4 (4) (2003) 155–166.
- [8] M. R. Kuhn, Are granular materials simple? An experimental study of strain gradient effects and localization., *Mech. of Mater.* 37 (5) (2005) 607–627.
- [9] M. R. Kuhn, Micro-mechanics of fabric and failure in granular materials, *Mech. of Mater.* 42 (9) (2010) 827–840.
- [10] M. R. Kuhn, K. Bagi, Specimen size effect in discrete element simulations of granular assemblies, *J. Eng. Mech.* 135 (6) (2009) 485–492.
- [11] A. Le Bouil, A. Amon, J.-C. Sangleboeuf, H. Orain, P. Bésuelle, Pierre, G. Viggiani, P. Chasle, J. Crassous, A biaxial apparatus for the study of heterogeneous and intermittent strains in granular materials, *Granular Matter* 16 (1) (2014) 1–8.
URL <http://dx.doi.org/10.1007/s10035-013-0477-x>
- [12] R. D. Mindlin, Micro-structure in linear elasticity, *Arch. Ration. Mech. Anal.* 16 (1964) 51–78.
- [13] R. D. Mindlin, Second gradient of strain and surface-tension in linear elasticity, *Int. J. Solids Struct.* 1 (4) (1965) 417–438.
- [14] A. Misra, P. Poorsolhjouy, Identification of higher-order elastic constants for grain assemblies based upon granular micromechanics, *Math. Mech. Complex Syst* 3 (3) (2015) 285–308.
- [15] A. Misra, P. Poorsolhjouy, Granular micromechanics based micromorphic model predicts frequency band gaps, *Continuum Mech. and Thermodyn.* 28 (1-2) (2016) 215–234.
- [16] D. Muir Wood, Heterogeneity and soil element testing, *Géotechnique Letters* 2 (July-September) (2012) 101–106.
- [17] W. Pabst, Micropolar materials, *Ceramics-Silikaty* 49 (3) (2005) 170–180.
- [18] L. Placidi, U. Andreaus, A. Della Corte, T. Lekszycki, Gedanken experiments for the determination of two-dimensional linear second gradient elasticity coefficients, *Zeitschrift für angewandte Mathematik und Physik* 66 (6) (2015) 3699–3725.
- [19] L. Placidi, U. Andreaus, I. Giorgio, Identification of two-dimensional pantographic structure via a linear d4 orthotropic second gradient elastic model, *J. Eng. Mech.* 103 (1) (2017) 1–21.
- [20] I. Vardoulakis, Lecture notes on Cosserat continuum mechanics with application to the mechanics of granular media, in: 3rd National Meeting on Generalized Continuum Theories and Applications, Thessaloniki, Greece, 2009.
- [21] H. Wolf, D. König, T. Triantafyllidis, Centrifuge model tests on sand specimen under extensional load, *Int. J. Numer. and Anal. Methods in Geomech.* 29 (1) (2005) 25–47.
URL <http://dx.doi.org/10.1002/nag.403>
- [22] Y. Yang, A. Misra, Micromechanics based second gradient continuum theory for shear band modeling in cohesive granular materials following damage elasticity, *Int. J. Solids Struct.* 49 (18) (2012) 2500–2514.